Theor Chem Acc (2000) 103:390–398
DOI 10.1007/s002149900045

Theoretical
Chemistry Accounts

Regular article

Diabatic and adiabatic potential-energy surfaces for azomethane photochemistry

Paola Cattaneo, Maurizio Persico

Dipartimento di Chimica e Chimica Industriale, Università di Pisa, via Risorgimento 35, I-56126 Pisa, Italy

Received: 18 February 1999 / Accepted: 12 April 1999 / Published online: 14 July 1999

Abstract. We propose an analytic form to represent the intersecting potential energy surfaces (PES) of the first two singlet states of azomethane. The aim is to run semiclassical simulations of photochemical events such as fragmentation and isomerization. The PES are based on ab initio calculations and corrected on the basis of available experimental data. We resort to a quasi-diabatic representation, suitable to deal with the S_0-S_1 conical intersection and to include the essential information about electronic couplings in a 2×2 effective hamiltonian matrix.

Key words: Azomethane – Photochemistry – Diabatic states – Conical intersections – Potential-energy surfaces

1 Introduction

Azomethane photochemistry is interesting for several reasons [1]. In the gas phase, excitation to the $n \rightarrow \pi^*$ S_1 state leads to fragmentation, with production of N_2 and two methyl radicals. In principle, the photofragmentation may take place by simultaneous and symmetric breaking of the two N—C bonds, or it may proceed through formation of the labile methyldiazenyl radical ($CH_3NN\cdot$), with all intermediate possibilities between these two limiting cases. Recent experiments have resulted in contrasting interpretations of the fragmentation mechanism [2–5]. The experimental results are consistent with a direct photodissociation on the S_1 surface, or a fast radiationless transition to lower states (T_1 or S_0). In solution, trans–cis photoisomerization occurs, while dissociation is almost completely inhibited.

Our aim is to run simulations of azomethane photochemistry, in order to uncover the mechanism of the gas-phase fragmentation and of the cage effect in solution. In view of the complexity of such a task, we shall rely on semiclassical dynamics, i.e. classical trajectories for the nuclear motion, with a quantum mechanical treatment of electronic transitions of the surface-hopping type [6, 7]. Such a study requires the determination of potential-energy surfaces (PES) and couplings between the electronic states. It is very convenient to obtain such information in the form of an effective Hamiltonian matrix in a quasi-diabatic basis of electronic states: this choice allows the cumbersome calculation of nonadiabatic couplings to be avoided, and solves the problem of representing the double cusps in the PES where conical intersections occur, as in the case of azomethane [8, 9].

The PES of azomethane have recently been explored by Liu et al. [10] and by ourselves [11]. In those studies, only some sections of the PES were determined and some geometry optimizations were performed in order to locate minima and transition states. Subsequently, we made a preliminary study of the photofragmentation dynamics, taking into account only the $C'N'N''C''$ skeletal coordinates [12]: our results indicate that the $S_1 \rightarrow S_0$ internal conversion (IC) is very fast, and so the role of the triplet states is probably not important. In this paper we present as complete a survey of the S_0 and S_1 PES as the dimensionality of the problem allows.

The construction of a PES for a polyatomic system with several internal coordinates undergoing large amplitude motions (bond twisting and dissociation) is a demanding task. A strategy must be devised in order to sample the interesting portions of the PES with single-point calculations, and a compromise must be reached between accuracy, completeness, and computational burden. We have run ab initio calculations in the framework of the configuration interaction by perturbation with multiconfigurational zeroth-order wavefunctions selected by a iterative process (CIPSI) algorithm [13–18] at about 270 different geometries. The ab initio results, in the form of a 2×2 Hamiltonian matrix in a quasidiabatic basis [11, 19, 20], have been fitted with analytic functions of the internal coordinates (see Sect. 2). This allowed us to perform a first characterization of the surfaces as functions of the skeletal coordinates only, and the preliminary simulations of Ref. [12]. In a second characterization, we added a dependence on the methyl internal coordinates, and we ran

Correspondence to: M. Persico
e-mail: mau@hermes.dcci.unipi.it

a restricted set of more accurate calculations with a triple-zeta basis set. Finally, we introduced corrections into the fitted PES, also taking into account the zero-point energies (ZPE) and some available experimental data (Sect. 3), in order to obtain the most suitable PES to run semiclassical simulations of the azomethane photochemistry. In Sect. 4 we present the most relevant potential-energy maps and critical points.

2 Ab initio calculations and fit of the PES

2.1 Complete active space self-consistent-field and CIPSI calculations

The first set of ab initio calculations was run with the 6-31G* basis set [21]. Geometry optimizations were performed at the complete active space self-consistent-field (CASSCF) level for some important minima in the S_0 and S_1 PES by means of the HONDO95 program [22]. The active space involved six electrons and six orbitals. The active molecular orbitals are the π and π^* pairs of N_2 and the p singly occupied orbitals of $CH_3\cdot$ at full dissociation. They correlate with the π, π^*, n (lone pairs) and σ^* (N—C bonds) orbitals of $CH_3NN\cdot$ and azomethane (see the correlation diagram of Fig. 1). The CASSCF results (Tables 1, 2) guided us in choosing a set of about 260 molecular geometries where single-point CIPSI calculations were performed. The five main skeletal coordinates ($\mathbf{Q}_{\text{skel}} \equiv \{R_1 = R_{\text{N}'\text{C}'},\ R_2 = R_{\text{N}''\text{C}''}, \theta_1 = \text{N}''\text{N}'\text{C}', \theta_2 = \text{N}'\text{N}''\text{C}'', \phi = \text{C}'\text{N}'\text{N}''\text{C}''\}$) were varied independently.

R_{NN} and the internal coordinates of the methyl groups ($\mathbf{Q}_{\text{met}}$) were adjusted so as to conform to the CASSCF values for the few skeletal geometries where an optimization was performed. For all other choices of $\mathbf{Q}_{\text{skel}}$, the coordinates R_{NN} and $\mathbf{Q}_{\text{met}}$ were smoothly interpolated as described in Ref. [11]. In this way, we were

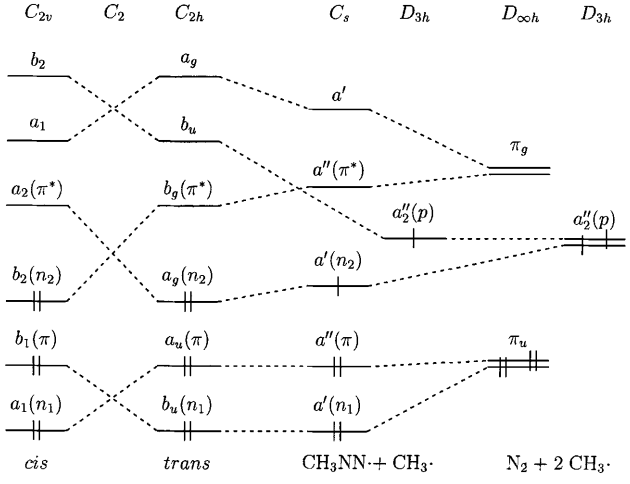

Fig. 1. Molecular orbital correlation diagram for the cis–trans isomerization and the fragmentation of azomethane. The *top line* indicates the point groups of isomers and fragments. A C_2 axis is ideally conserved in the isomerization pathway (torsion) and a reflection plane in the bond dissociations

Table 1. Energies of critical points of the potential-energy surface (*PES*) (kcal/mol), relative to *trans*-azomethane. Complete active space self-consistent-field (*CASSCF*) 6-31G* calculations with full geometry optimization. Configuration interaction by perturbation with multiconfigurational zeroth-order wavefunctions selected by an iterative process (*CIPSI*) 6-311G** calculations at geometries optimized by means of the first approximation analytic PES (see text) and zero-point energy (*ZPE*) computed on the same PES

Molecule and state	Method and reference	ΔE	ΔE + ZPE
cis-CH_3NNCH_3[a], S_0	CASSCF	11.0	
	CIPSI	14.8	
	[27]	11.4	11.2
	[28]	9.3	9.0
	Exp. [26]		8.0
Rotamer, min. S_1	CASSCF	95.3	
	CIPSI[b]	74.2	
	[10]	78.7	
$CH_3NN\cdot(^2A') + CH_3\cdot$	CASSCF	53.0	
	CIPSI	60.2	54.3
	[27]	53.7	46.3
	[10]	56.9	51.5
	[28]	51.2	47.8
	Exp. [31]		50.9
$N_2 + 2CH_3\cdot$	CASSCF	10.1	
	CIPSI	48.6	37.5
	[27, 30]	35.8	22.1
	[10]	34.2	22.2
	Exp. [29]	43.1	31.6
Transition state for symmetric dissociation[c]	CASSCF	47.8	
	CIPSI	75.2	71.6
	[27]	60.7	53.6
	[10]	52.2	44.2
	[28]	64.7	59.5

[a] Eclipsed conformation for both methyl groups
[b] Fixed torsion angle $\text{C}'\text{N}'\text{N}''\text{C}'' = 90°$
[c] Transition state for the simultaneous breaking of both N—C bonds in *trans*-azomethane, with C_{2h} symmetry constraint

able to describe all the interesting regions of the potential hypersurfaces without considering their explicit dependence on the $\mathbf{Q}_{\text{met}}$, which were roughly optimized as functions of the other coordinates. Of course, in this "contracted-methyl" treatment, we also neglected the difference between S_0 and S_1 as to the equilibrium $\mathbf{Q}_{\text{met}}$. Finally, we chose eight representative sets of $\mathbf{Q}_{\text{skel}}$, which were held fixed while varying R_{NN}: on the basis of these results we established a harmonic dependence of the potentials on R_{NN}, the equilibrium distance and force constant being functions of the $\mathbf{Q}_{\text{skel}}$.

At each geometry we performed a state-averaged CASSCF and we computed the eigenvectors of the average density matrix natural orbitals to be used as one-electron functions in the CIPSI-quasi degenerate perturbation theory (QDPT) [20] calculations. CIPSI is a multireference perturbation CI characterized by the individual selection of the determinants which span the zeroth-order wavefunctions [13–18]. CIPSI calculations were run in the QDPT framework so as to obtain second-order corrected diagonal and off-diagonal matrix elements of the electronic Hamiltonian in the quasi-diabatic basis $|\eta_I\rangle$: $H_{IJ} = \langle \eta_I | \hat{\mathscr{H}}_{\text{el}} | \eta_J \rangle$ The transformation of the eigenvectors of $\hat{\mathscr{H}}_{\text{el}}$ in the zeroth-order subspace $\mathscr{S}$ to quasidiabatic wavefunctions was done by

Table 2. Optimized geometries. Distances (bohr), angles (degree) and energies (kcal/mol) relative to *trans*-azomethane

Molecule and state	Method	R_{NN}	$R_{N'C'}$ $R_{N''C''}$	$\angle N''N'C'$ $\angle N'N''C''$	$\angle C'N'N''C''$	ΔE	$\Delta E + ZPE$
trans-CH_3NNCH_3[a], S_0	CASSCF	2.372	2.772	112.4	180.0	0.0	
	Final fit	2.379	2.765	109.9	180.0		0.0
	Liu et al.[f]	2.368	2.767	111.7	180.0	0.0	0.0
	Exp. [32]	2.356	2.801	112.3	180.0		
	Exp. [33]	2.370	2.785	111.9	180.0		
cis-CH_3NNCH_3[a], S_0	CASSCF	2.375	2.765	124.3	0.0	11.0	
	Final fit	2.343	2.974	117.2	0.0		7.9
	Exp. [34]	2.370	2.797	119.3	0.0		
Rotamer[b], S_0	CASSCF	2.451	2.782	122.9	90.0	69.7	
	Final fit	2.458	2.729	122.3	90.0		66.9
Invertomer[c], S_0	CASSCF	2.355	2.797	115.2		55.3	
			2.666	180.0			
	Final fit	2.417	2.852	112.4			56.0
			2.588	180.0			
Rotamer, min. S_1	CASSCF	2.391	2.736	125.0	119.8	95.3	
	Final fit	2.437	2.751	120.8	130.8		69.3
	Liu et al.[g]	2.392	2.738	124.9	120.8	78.7	
Conical intersection	Final fit	2.327	2.647	120.3	93.8		73.7
	Liu et al.[h]	2.423	2.770	115.6	92.8	73.8	
			2.729	132.0			
$CH_3NN\cdot(^2A') + CH_3\cdot$	CASSCF	2.370	2.679	116.5		53.0	
	Final fit	2.276	2.824	118.5			48.4
	Liu et al.[f]	2.156	2.848	125.6		56.9	51.5
$CH_3NN\cdot(^2A'') + CH_3\cdot$	CASSCF	2.228	2.682	179.0		88.1	
	Final fit	2.324	2.766	180.0			75.9
$N_2 + 2CH_3\cdot$	CASSCF	1.969				10.1	
	Final fit	2.115					31.6
	Exp. [35]	2.074					
Transition state for symmetric dissociation[d]	CASSCF	2.171	3.868	108.6	0.0	47.8	
	Final fit	2.221	4.133	114.7	0.0		64.9
	Liu et al.[f]	2.130	4.207		0.0	52.2	44.2
Transition state for $CH_3NN\cdot$ dissociation[e]	Final fit	2.169	3.752	120.2			59.5
	Liu et al.[f]	2.105	3.358	121.8		65.9	58.2

[a] Eclipsed conformation for both methyl groups
[b] Twisted geometry, with the constraint $\angle C'N'N''C'' = 90°$
[c] Semilinear geometry, with the constraint $\angle N'N''C'' = 180°$
[d] Transition state for the simultaneous breaking of both N—C bonds in *trans*-azomethane, with C_{2h} symmetry constraint
[e] Transition state for the dissociation of $CH_3NN\cdot$, with $CH_3\cdot$ energy added
[f] MP2 geometries and QCISD(T) energies with 6-311G(2d,p) basis [10]
[g] Single-state CASSCF geometries and energies with DZP basis [10]
[h] State-average CASSCF geometries and energies with DZP basis [10]

the method of diabatic templates described in Refs. [11, 19, 20]. The diabatic states coincide with the adiabatic ones whenever a C_2 axis or a reflection plane is present. $|\eta_1\rangle$ is the ^1A state and $|\eta_2\rangle$ the ^1B state along the N—N torsion pathway. They are $^1A'$ and $^1A''$, respectively, in the case of in-plane dissociation, and they correlate with the $^2A'$ and $^2A''$ states of $CH_3NN\cdot$.

The subspace $\mathscr{S}$ was selected at each geometry so as to guarantee uniform quality for all calculations. This can be accomplished by an iterative selection procedure [17] which aims at obtaining a given target value of the square norm σ of the first-order correction to the wavefunction at all geometries and for all electronic states: $\sigma = 0.15$ was imposed in the fourth and last CIPSI step. We adopted the Epstein–Nesbet partition of the CI Hamiltonian and we applied the extrapolation algorithm of Ref. [16].

2.2 Fit of the diagonal matrix elements H_{II}

In a first step the matrix elements of **H** were considered only as functions of the $\mathbf{Q}_{skel}$ and R_{NN}. The fitting function for the diagonal matrix elements was in the form

$$\begin{aligned} H_{II}(R_{NN}, R_1, R_2, \theta_1, \theta_2, \phi) &= P_0 + P_1 R_{CC}^{-12} + U_{NN}(R_{NN}, R_1, R_2, \theta_1, \theta_2, \phi) \\ &\quad + A(R_1, \theta_1) + A(R_2, \theta_2) \\ &\quad + \left\{ \sum_{n=0}^{3} B_n(\theta_1, \theta_2, \phi)[Y^n(R_1) + Y^n(R_2)] \right. \\ &\quad + \sum_{n=0}^{3} [C_n(\theta_1, \theta_2, \phi) Y^n(R_1) + C_n(\theta_2, \theta_1, \phi) Y^n(R_2)] \end{aligned}$$

$$+ Y(R_1)Y(R_2)\sum_{n=0}^{1} D_n(\theta_1,\theta_2,\phi) \times [Y^n(R_1)+Y^n(R_2)]\Big\}X(R_1)X(R_2) \quad (1)$$

$$A(R_i,\theta_i) = \exp(-P_2R_i)\ \sum_{k=0}^{3}\sum_{l=0}^{2} A_{kl}\ R_i^k\ \cos(l\theta_i) \quad (2)$$

$$\begin{aligned} B_n(\theta_1,\theta_2,\phi) &= B_{n,1} + B_{n,2}W_1(\theta_1,\theta_2) + B_{n,3}W_1(2\theta_1,2\theta_2) \\ &\quad + \cos\phi[B_{n,4}W_2(\theta_1,\theta_2) + B_{n,5}W_4(\theta_1,\theta_2)] \\ &\quad + \cos 2\phi[B_{n,6}W_4(\theta_1,\theta_2) \\ &\quad + B_{n,7}W_4(2\theta_1,2\theta_2) + B_{n,8}W_4(4\theta_1,4\theta_2)] \\ &\quad + B_{n,9}\cos 3\phi W_2(\theta_1,\theta_2) \\ &\quad + B_{n,10}\cos 4\phi W_4(2\theta_1,2\theta_2) \end{aligned} \quad (3)$$

$$\begin{aligned} C_n(\theta_i,\theta_j,\phi) &= C_{n,1}\ \cos\theta_i + C_{n,2}\cos 2\theta_i \\ &\quad + C_{n,3}\ \cos\ \phi\ \sin\ 2\theta_i\ \sin\ \theta_j \end{aligned} \quad (4)$$

$$\begin{aligned} D_n(\theta_1,\theta_2,\phi) &= D_{n,1} + D_{n,2}W_3(\theta_1,\theta_2) \\ &\quad + \cos\phi[D_{n,3}\ W_2(\theta_1,\theta_2) + D_{n,4}W_5(\theta_1,\theta_2)] \\ &\quad + \cos 2\phi\ [D_{n,5}W_4(2\theta_1,2\theta_2) + D_{n,6}W_4(4\theta_1,4\theta_2)] \\ &\quad + D_{n,7}\cos 3\phi W_2(\theta_1,\theta_2) \\ &\quad + D_{n,8}\cos 4\phi W_4(2\theta_1,2\theta_2) \end{aligned} \quad (5)$$

$$W_1(\theta_1,\theta_2) = \cos\theta_1\ \cos\theta_2 \quad (6)$$

$$W_2(\theta_1,\theta_2) = \sin\theta_1\ \sin\theta_2 \quad (7)$$

$$W_3(\theta_1,\theta_2) = \cos\theta_1 + \cos\theta_2 \quad (8)$$

$$W_4(\theta_1,\theta_2) = 1 - \cos\theta_1 - \cos\theta_2 + \cos\theta_1\ \cos\theta_2 \quad (9)$$

$$W_5(\theta_1,\theta_2) = \sin 2\theta_1\ \sin\theta_2 + \sin\theta_1\ \sin 2\theta_2 \quad (10)$$

$$\begin{aligned} X(R_i) &= \exp(-P_3R_i) \quad \text{for } R_i \le P_4 \\ X(R_i) &= \exp[-P_3R_i - P_3(R_i-P_4)^2] \quad \text{for } R_i > P_4 \end{aligned} \quad (11)$$

$$Y(R_i) = (R_i - P_5)X(R_i) \quad (12)$$

$$\begin{aligned} U_{\mathrm{NN}} &= F_1(R_1,R_2,\theta_1,\theta_2,\phi) \\ &\quad \times [R_{\mathrm{NN}} - F_2(R_1,R_2,\theta_1,\theta_2,\phi)]^2 \end{aligned} \quad (13)$$

$$\begin{aligned} F_n(R_1,R_2,\theta_1,\theta_2,\phi) &= F_{n,1} + \sum_{i=1}^{2}[F_{n,2} + F_{n,3}(R_i - P_5)]\exp[-F_{n,4}R_i] \\ &\quad - [2F_{n,2} + F_{n,3}(R_1+R_2-2P_5)]\exp[-F_{n,4}(R_1+R_2)/2] \\ &\quad + [F_{n,5} + F_{n,6}\cos\phi W_2(\theta_1,\theta_2) \\ &\quad + F_{n,7}\cos 2\phi W_3(\theta_1,\theta_2) + F_{n,8}(R_1+R_2-2P_5)/2] \\ &\quad \times \exp[-F_{n,9}(R_1+R_2-2P_5)/2]\ . \end{aligned} \quad (14)$$

$P_k, A_{kl}, B_{nk}, C_{nk}, D_{nk}$ and F_{nk} are constant parameters to be determined separately for the two electronic states. The function (Eq. 1) was devised so as to obey some fundamental symmetry rules which are stated here for the diagonal as well as for the off-diagonal matrix elements.

1. **H** cannot depend on the dihedral angle ϕ at semilinear geometries:

$$\frac{\partial^n H_{IJ}}{\partial\phi^n} = 0 \quad \text{for } \theta_1 = \pi \text{ or } \theta_2 = \pi \text{ (all } n \ge 1)\ . \quad (15)$$

2. The diagonal matrix elements are even functions of ϕ and of $\phi - \pi$:

$$\frac{\partial^n H_{II}}{\partial\phi^n} = 0 \quad \text{for } \phi = 0 \text{ or } \phi = \pi \text{ (odd } n \ge 1)\ . \quad (16)$$

3. The off-diagonal matrix element is an odd function of ϕ and of $\phi - \pi$:

$$\frac{\partial^n H_{12}}{\partial\phi^n} = 0 \quad \text{for } \phi = 0 \text{ or } \phi = \pi \text{ (even } n \ge 0)\ . \quad (17)$$

Moreover,

$$H_{12} = 0 \quad \text{for } \theta_1 = \pi \text{ or } \theta_2 = \pi\ . \quad (18)$$

4. Reflection symmetry of C″ about the C′N′N″ plane and of C′ about C″N″N′:

$$\frac{\partial^n H_{II}}{\partial\theta_k^n} = 0 \quad \text{for } \phi = \pi/2 \text{ and } \theta_k = \pi \text{ (odd } n \ge 1) \quad (19)$$

$$\frac{\partial^n H_{12}}{\partial\theta_k^n} = 0 \quad \text{for } \phi = \pi/2 \text{ and } \theta_k = \pi \text{ (even } n \ge 0)\ . \quad (20)$$

In the H_{II} functions all terms vanish for large R_1 and R_2, with the exception of P_0 and U_{NN}. The latter also vanishes when $R_{\mathrm{NN}} = F_{2,1}$, the equilibrium distance of N_2. We set $P_0 = 0$ for the ground-state diabatic potential H_{11}, so that all energies are referred to the separated fragments $N_2 + 2CH_3\cdot$. The P_0 parameter for H_{22} sets the energy gap between the two diabatic surfaces. P_5 is a reference distance, set for convenience to 2.8 bohr in order to avoid very large values of the powers of $(R_i - P_5)$.

The U_{NN} term carries the only explicit dependence on R_{NN}, in the form of a quadratic function. The force constant $2F_1$ and the equilibrium distance F_2 are functions of the $\mathbf{Q}_{\mathrm{skel}}$, each depending on nine $F_{n,k}$ parameters which are determined on the basis of calculations run at selected skeletal geometries with variable R_{NN}. At all other $\mathbf{Q}_{\mathrm{skel}}$ points R_{NN} was not varied, rather it was chosen close to its equilibrium value. Therefore, in the next steps of the fitting, the $F_{n,k}$ parameters are held fixed.

When just one of the R_i, say R_1, is large, H_{II} reduces to $U_{\mathrm{NN}} + A(R_2,\theta_2)$, which is the potential for a separate $CH_3NN\cdot$ fragment. The other terms are only important for the united azomethane molecule. All the parameters yet to be determined were optimized in order to fit 189 ab initio values in the weighted-least-squares sense, with

the lowest weights for the highest energies corresponding to the least accessible portions of the PES. At this stage, several terms contained in the A, B_n, C_n and D_n functions were eliminated, setting their parameters to zero, because their contribution was found to be not important. In total, we had 86 parameters for each state (besides P_0 and P_5), and this led to standard deviations of 1.99 and 2.26 kcal/mol for S_0 and S_1 respectively. The largest errors were concentrated in the repulsive parts of the potentials.

2.3 Fit of the off-diagonal matrix element H_{12}

The analytic function for the off-diagonal matrix element H_{12} was simpler than that of H_{II}, because there are many less ab initio values to be fitted: in fact, at all symmetric geometries (C_2 or C_s) H_{12} vanishes, and this is implicit in the form of the fitting function. We have

$$\begin{aligned} H_{12}(R_1,R_2,\theta_1,\theta_2,\phi) &= G_1(\phi)\ W_6(\theta_1,\theta_2) \\ &\quad + G_2(\phi)\ W_6(2\theta_1,2\theta_2) \\ &\quad + [G_3(\phi)+G_4(\phi)\ W_6(\theta_1,\theta_2)]\ [Z(R_1)-Z(R_2)] \\ &\quad + G_5(\phi)\ [Z^2(R_1)-Z^2(R_2)] \\ &\quad + G_6(\phi)\ (R_1-R_2)\ \exp[-S_1(R_1-R_2)^2]\ , \end{aligned} \tag{21}$$

where

$$G_n(\phi) = G_{n,1}\ \sin\ \phi + G_{n,2}\ \sin\ 2\phi + G_{n,3}\ \sin\ 3\phi \tag{22}$$

$$W_6(\theta_1,\theta_2) = \cos\theta_1 - \cos\theta_2 \tag{23}$$

$$Z(R_i) = (R_i - S_2)\exp[-S_3 R_i] \tag{24}$$

Twenty-one G_{nk} and S_k parameters were optimized. The standard deviation was 1.23 kcal/mol. Plots of the H_{12} function show that it can reach rather large values in scarcely accessible, high-energy regions of the PES, where no ab initio calculations were done. We therefore decided to damp down all H_{12} values above $H_{\rm cut} =$ 8 kcal/mol so that it could never exceed $H_{\rm max} = 12$ kcal/mol. This was done by replacing $|H_{12}| > H_{\rm cut}$ with

$$\begin{aligned} |H'_{12}| &= H_{\rm cut} + [H_{\rm max} - H_{\rm cut}] \\ &\quad \times [1 - \exp[-(|H_{12}| - H_{\rm cut})/(H_{\rm max} - H_{\rm cut})]] \end{aligned} \tag{25}$$

2.4 Exchange of the methyl groups

Until at least one of the two N—C bonds is close to its equilibrium length, one may safely use the analytic functions defined in Sects. 2.1–2.3, with the identifications $R_1 = R_{\rm N'C'}, R_2 = R_{\rm N''C''}, \theta_1 = {\rm N''N'C'}$ and $\theta_2 = {\rm N'N''C''}$; however, when both bonds are significantly stretched, one cannot ignore the possibility of methyl exchange, i.e. that $R_{\rm N'C''} < R_{\rm N'C'}$ and/or $R_{\rm N''C'} < R_{\rm N''C''}$. The problem is to switch smoothly from $H_{IJ}(R_{\rm NN}, R_{\rm N'C'}, R_{\rm N''C''}, {\rm N''N'C'},\ {\rm N'N''C''}, {\rm C'N'N''C''})$ to $H_{IJ}(R_{\rm NN},\ R_{\rm N'C''},\ R_{\rm N''C'},\ {\rm N''N'C''},\ {\rm N'N''C'},\ -{\rm C'N'N''C''})$. To this aim we define a parameter ρ, which is positive in the regions where we want $R_1 = R_{\rm N'C'}, R_2 = R_{\rm N''C''}$ etc and is negative where $R_1 = R_{\rm N'C''}, R_2 = R_{\rm N''C'}$, etc:

$$\begin{aligned} \rho &= \exp(-R_{\rm N''C'}/R_{\rm N'C'}) - \exp(-R_{\rm N'C'}/R_{\rm N''C'}) \\ &\quad + \exp(-R_{\rm N'C''}/R_{\rm N''C''}) - \exp(-R_{\rm N''C''}/R_{\rm N'C''})\ . \end{aligned} \tag{26}$$

The Hamiltonian matrix elements actually used in the dynamics are weighted averages:

$$\begin{aligned} H_{IJ} &= W(\rho) \\ &\quad \times H_{IJ}(R_{\rm NN}, R_{\rm N'C'}, R_{\rm N''C''}, {\rm N''N'C'}, {\rm N'N''C''}, {\rm C'N'N''C''}) \\ &\quad + [1 - W(\rho)] H_{IJ}(R_{\rm NN}, R_{\rm N'C''}, R_{\rm N''C'}, {\rm N''N'C''}, \\ &\qquad {\rm N'N''C'}, -{\rm C'N'N''C''})\ , \end{aligned} \tag{27}$$

where

$$\begin{aligned} W(\rho) &= 0 && \text{for } \rho \le -1 \\ W(\rho) &= \frac{1}{2} + \frac{3\rho}{4} - \frac{\rho^3}{4} && \text{for } -1 < \rho < 1 \\ W(\rho) &= 1 && \text{for } \rho \ge 1 \end{aligned} \tag{28}$$

2.5 Methyl internal coordinates

In order to introduce a reasonable but not detailed dependence of the potential on the methyl coordinates, we ran a few supplementary calculations, for *cis*- and *trans*-azomethane and $CH_3\cdot$, varying the six C—H bond lengths (r_i), the six NCH and the six HCH bond angles (α_i and β_i, respectively), the six HCHH dihedral angles (γ_i) and the two NNCH torsion angles (τ_k). Notice that, for the sake of simplicity, each τ_k angle is determined by the position of only one H atom per methyl group, arbitrarily chosen. We then added to the diagonal matrix elements (Sect. 2.2) a contribution for each methyl group, of the form

$$\begin{aligned} U_{\rm met} &= V_\tau(R_k,\theta_k)\frac{1-\cos 3\tau_k}{2} \\ &\quad + \frac{K_{\rm CH}(R_k)}{2}\sum_{i=1}^{3}[r_i - r_0(R_k)]^2 \\ &\quad + \frac{K_\alpha(R_k)}{2}\sum_{i=1}^{3}[\alpha_i - \alpha_0(R_k)]^2 \\ &\quad + \frac{K_\beta(R_k)}{2}\sum_{i=1}^{3}[\beta_{ij} - \beta_0(R_k)]^2 \\ &\quad + \frac{K_\gamma(R_k)}{2}\sum_{i=1}^{3}[1 - \cos(\gamma_i - \gamma_0(R_k))] \end{aligned} \tag{29}$$

plus the H—H repulsion term:

$$U_{\rm rep} = K_{\rm rep}\sum_{i,j=1}^{3}\frac{1}{r_{ij}^{12}} \tag{30}$$

Here the force constants $K_{\rm CH}, K_\alpha, K_\beta$ and K_γ, and the equilibrium values r_0, α_0, β_0 and γ_0 are functions of the

N—C bond length R_k. For each of these quantities we interpolate smoothly between the values determined for *trans*-azomethane and the isolated methyl radical. If $K(R_k)$ is the constant to be interpolated, we assume

$$K(R_k) = K_{\text{met}} + f(R_k)\ (K_{\text{azm}} - K_{\text{met}})\ . \tag{31}$$

$f(R_k)$ goes from 1 to 0 as the N—C bond length R_k increases from its equilibrium value to a large distance:

$$f(R) = 1 \quad \text{for } R \le R_{\min}$$

$$f(R) = 2X^3 - 3X^2 + 1,$$

$$X = \frac{R - R_{\min}}{R_{\max} - R_{\min}} \text{ for } R_{\min} < R < R_{\max}$$

$$f(R) = 0 \quad \text{for } R \ge R_{\max}$$

with $R_{\min} = 2.77$ bohr and $R_{\max} = 6.61$ bohr.
The torsional barrier V_τ also depends on the NNC bond angle θ_k

$$V_\tau(R_k, \theta_k) = V_0\ f(R_k)\ (1 + \cos\theta_k) \tag{33}$$

and so the torsional potential vanishes at semilinear geometries ($\theta_k = \pi$). $V_0 = 2.60$ and -5.02 kcal/mol was determined for S_0 and S_1 respectively, on the basis of the eclipsed versus staggered energy differences for both methyls in *trans*-azomethane. The H—H repulsion constant K_{rep} was evaluated from the energy difference between conformers of *cis*-azomethane, after deducting the torsional contribution. Finally, once we had fixed V_0 and K_{rep}, we fitted a few ab initio energy values obtained for trans-azomethane and $CH_3\cdot$ with variable bond lengths and angles, to determine the force constants and equilibrium values K_{azm} and K_{met} of Eq. (31).

3 Higher-accuracy corrections

In order to improve the accuracy of the PES, we ran a few more CIPSI calculations with higher standards:

1. Triple-zeta basis set with polarization functions also on the H atoms, 6-311G** [23].
2. One-electron functions for the CI generated by means of preliminary CIPSI calculations and diagonalization of the perturbed single-particle density matrix of the target state [24].
3. Single-state CIPSI calculations (Epstein–Nesbet baricentric partition) with more exacting thresholds ($\sigma = 0.10$) in the final step, which requires up to 29500 determinants for the zeroth-order wavefunction.

Calculations were run at geometries optimized according to the analytic PES of Sect. 2; however, in order to offset the effect of some arbitrariness in the definition of the U_{met} potential (Sect. 2.5), we reoptimized the methyl coordinates by CASSCF. In this way we determined a few important energy differences, some of which have also been determined experimentally (Table 1).

The computed vertical transition energies for *trans*- and *cis*-azomethane are 88.6 and 82.4 kcal/mol, respectively: these values roughly match the broad absorption maxima at $\lambda \simeq 355$ and 370 nm, respectively [25]. The $^2A' - ^2A''$ transition energy for $CH_3NN\cdot$ turns out to be 50.2 kcal/mol (570 nm): no experimental data are available for this radical. The S_1 state has a twisted minimum, which was provisionally optimized with the constraint $\phi = 90°$, and was found at 74.2 kcal/mol above the trans isomer. At the same geometry, the energy gap with S_0 is only 3.8 kcal/mol.

The cis–trans energy difference is estimated from experiment to be about 8 kcal/mol [26]: we calculate 14.8 kcal/mol, to be compared with other theoretical values of 11.2 [27] and 9.3 [28].

The full fragmentation energy to $N_2 + 2CH_3\cdot$ has been accurately determined on the basis of thermochemical data [29] to be 31.6 kcal/mol. Including the ZPE (computed on the basis of the first fit of the PES), we obtain 37.5 kcal/mol (Liu et al. [10] give 22.2 and Hu and Schaefer [27, 30] give 22.1). For the N—C bond dissociation thermal reaction, an activation energy of 50.9 kcal/mol has been measured at 540–610 K [31]: assuming that no barrier is present along the reaction path, as found by our calculations, this can be taken as an indication of the energy difference of $CH_3NN\cdot + CH_3\cdot$ versus *trans*-azomethane. Our computed value, including ZPE, is 54.3 kcal/mol (compare with Hu and Schaefer [27] 46.3 kcal/mol, Liu et al. [10] 51.5 kcal/mol and Vrábel et al. [28] 47.8 kcal/mol). A substantial barrier is instead found along the symmetric (D_{2h}) dissociation path for both N—C bonds, starting from *trans*-azomethane: with ZPE, 71.6 kcal/mol above the reagent (that is 34.1 kcal/mol above $N_2 + 2CH_3\cdot$). According to Hu and Schaefer [27] and Liu et al. [10] the barrier is substantially lower, 53.6 and 44.2 kcal/mol, respectively: notice that their calculations underestimate the fragmentation energy, while we overestimate it; Vrábel et al. [28] give 59.5 kcal/mol.

Our computed values are in overall agreement with other experimental and theoretical results. The most important discrepancies, in view of the use of these PES in simulations of azomethane photochemistry, are the overestimation of the cis–trans energy difference, which probably includes a slight deformation of the rather flat S_1 PES, and the overestimation of the full fragmentation energy and of the relative barrier. Therefore, we introduced corrections to the analytic PES of Sect. 2 with the aim of producing an effective **H** matrix suitable for semiclassical simulations. In detail, we wanted

1. To adapt the analytic PES to the results of the higher-quality calculations reported in this section; ZPE corrections were also included, as they would not be taken into account explicitly in a classical trajectory treatment.
2. To further correct the PES according to the experimental value for the full fragmentation energy: half of the required correction (-5.9 kcal/mol) was applied to the symmetric dissociation barrier height.
3. To correct the cis–trans energy difference by -6.8 kcal/mol and the rotamer energy by half of this value.
4. To leave unchanged both the equilibrium geometries and the excitation energies, which are satisfactory

and/or cannot be improved substantially on the basis of available experimental data.

The correction takes the form of two additional terms in the diabatic potentials H_{II}. The first term is

$$U^{(1)}_{\text{add}}(R_1, R_2) = T_1\{f(R_1)[1 - f(R_2)] + f(R_1)[1 - f(R_2)]\} \quad (34)$$

with $f(R)$ as defined in Eq. (32), but $R_{\min} = 2.8$ bohr and $R_{\max} = 4$ bohr. The second term is

$$U^{(2)}_{\text{add}}(R_1, R_2, \phi, \theta_1, \theta_2) = [T_2 + T_3 \cos\phi W_2(\theta_1, \theta_2) + T_4 \cos 2\phi W_4(\theta_1, \theta_2)] f(R_1) f(R_2) \quad (35)$$

with $R_{\min} = 2.8$ bohr and $R_{\max} = 7.6$ bohr. The parameters T_n were optimized so as to satisfy the requirements outlined above.

Parameter files and Fortran subprograms for the calculation of the H_{IJ} matrix elements can be obtained from the authors.

4 Potential-energy maps and critical points

The results of several geometry optimizations, both at CASSCF level and with our final analytic PES, are given in Table 2. We also located the most important transition states and the lowest point of the crossing seam between the S_0 and S_1 surfaces. The saddle points for the symmetric dissociation of both N—C bonds and for the cis–trans isomerization by torsion are actually not true transition states, as the Hessian matrix has more than one negative eigenvalue: they were obtained by imposing symmetry constraints in the optimization (C_{2h} and C_2, respectively).

Some sections of the PES are shown in Figs. 2–7, which are contour maps obtained with full optimization of all geometrical parameters save two independent variables, using the fitted analytic PES.

In the ground state the cis–trans isomerization may follow either the in-plane inversion or the double-bond torsion pathway. The former is clearly preferred (see Table 2). Figure 2 illustrates the isomerization (by inversion) and the single-bond dissociation reactions. Both *trans*- and *cis*-azomethane dissociate without going through a transition state. The activation energy for nitrogen inversion, 56.0 kcal/mol, is higher than the dissociation energy, 48.4 kcal/mol, which is why thermal fragmentation takes place instead of isomerization. In Fig. 3 one may compare one- and two-bond dissociation, starting with *trans*-azomethane. While the full fragmentation products, $N_2 + 2CH_3\cdot$, are more stable than $CH_3NN\cdot + CH_3\cdot$, the simultaneous dissociation of both N—C bonds is not favoured: with the constraint of D_{2h} symmetry, one finds a barrier of 64.9 kcal/mol. While this value may still be slightly overestimated (see Sect. 3), the difference with the single-bond dissociation energy is large enough (16.5 kcal/mol) to guarantee an unsymmetrical, if not sequential, bond breaking.

The ground-state ($^2A'$) PES of $CH_3NN\cdot$ is shown in Fig. 4 as a function of R_{NC} and of the NNC angle. The

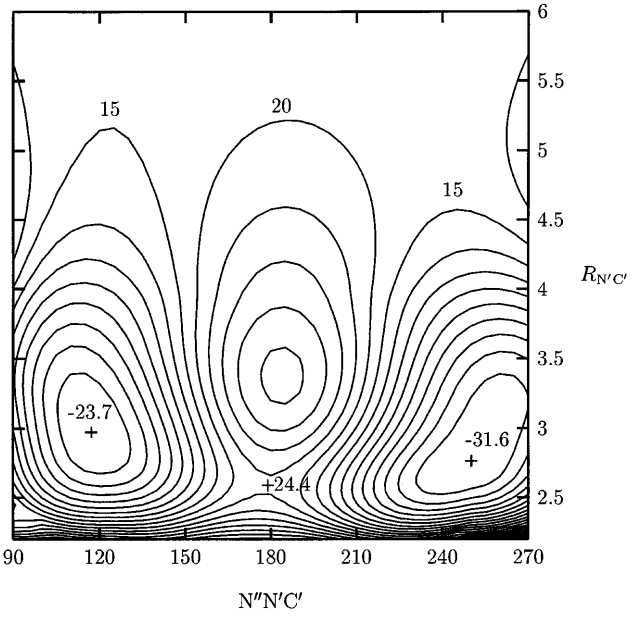

Fig. 2. Potential energy map for S_0 ($^1A'$). One NNC angle and the corresponding R_{NC} distance are varied independently, all other coordinates are optimized. The distance between two contour lines is 5 kcal/mol, all energies being relative to $N_2 + 2CH_3\cdot$. The locations and energies of some critical points are shown on the map. Distances in bohr, angles in degree

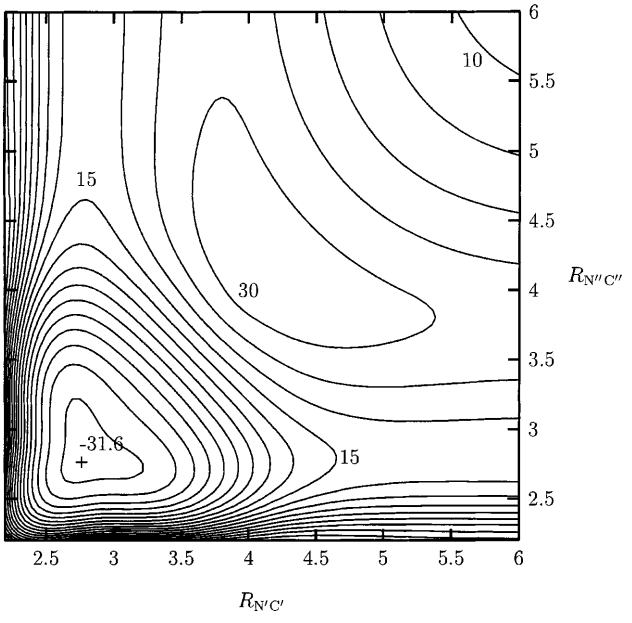

Fig. 3. Potential energy map for S_0 ($^1A'$). Both R_{NC} distances are varied independently, all other coordinates are optimized with the constraint CNNC = 180° (transoid geometries). The distance between two contour lines is 5 kcal/mol, all energies being relative to $N_2 + 2CH_3\cdot$. The locations and energies of some critical points are shown on the map. Distances in bohr

transition state for the dissociation to $N_2 + CH_3\cdot$ is 11.1 kcal/mol above the minimum (Liu et al. [10], with ZPE, give 6.7 kcal/mol; Hu and Schaefer et al. [30] give 2.3 kcal/mol). The equilibrium geometry is bent in the

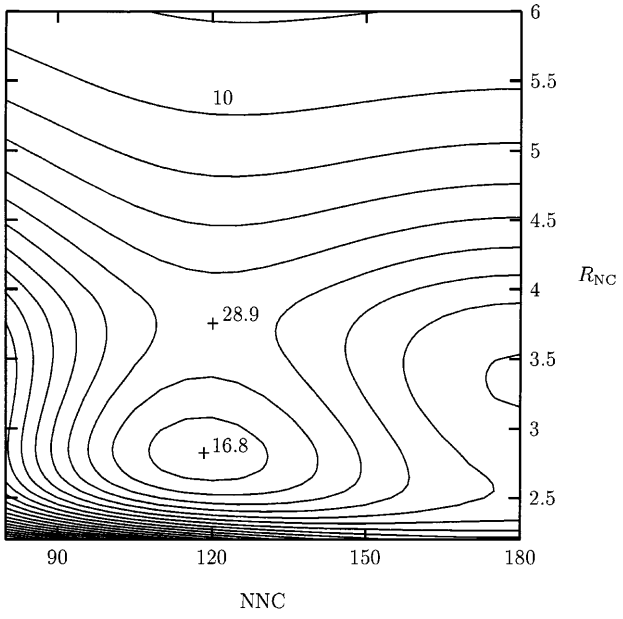

Fig. 4. Potential energy map for the ground state of $CH_3NN\cdot$ ($^2A'$). The NNC angle and the R_{NC} distance are varied independently, all other coordinates are optimized. The distance between two contour lines is 5 kcal/mol, all energies being relative to $N_2 + 2CH_3\cdot$. The locations and energies of some critical points are shown on the map. Distances in bohr, angles in degree

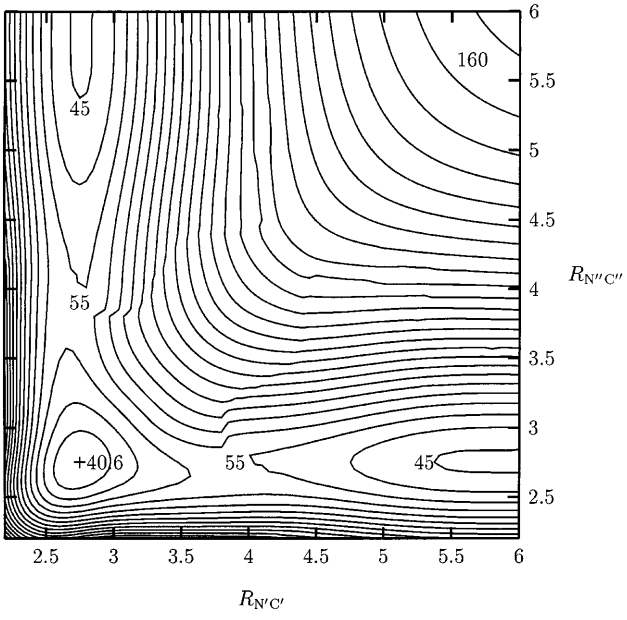

Fig. 5. Potential energy map for S_1 ($^1A''$). Both R_{NC} distances are varied independently, all other coordinates are optimized. The distance between two contour lines is 5 kcal/mol, all energies being relative to $N_2 + 2CH_3\cdot$. The locations and energies of some critical points are shown on the map. Distances in bohr, angles in degree

ground state. In contrast the $^2A''$ excited state prefers an almost linear geometry, where it becomes degenerate with $^2A'$.

The S_1 PES of *trans*-azomethane is shown in Fig. 5 as a function of the R_{NC} bond lengths. The PES has a

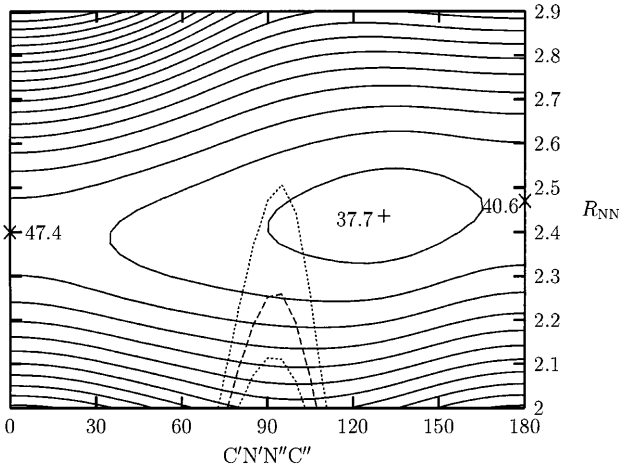

Fig. 6. Potential energy map for the ^1B diabatic state. The CNNC dihedral angle and the R_{NN} distance are varied independently, all other coordinates are optimized with C_2 symmetry constraints. The distance between two contour lines is 5 kcal/mol, all energies being relative to $N_2 + 2CH_3\cdot$. The locations and energies of some critical points are shown on the map. The *dashed line* indicates the crossing seam with the ^1A surface. The *dotted lines* enclose the region where $|\Delta E(S_0 - S_1)| < 5$ kcal/mol. Distances in bohr, angles in degree

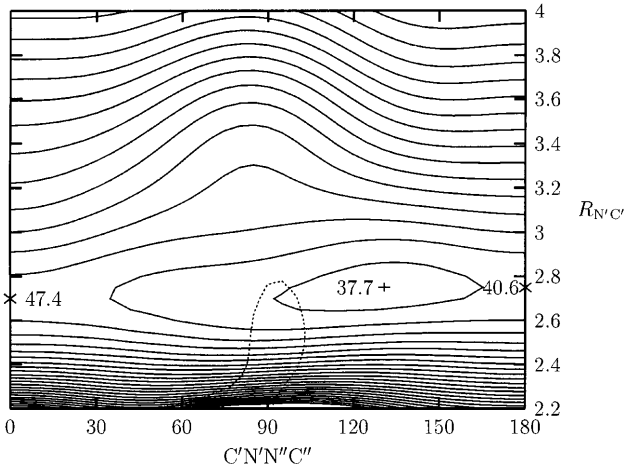

Fig. 7. Potential energy map for the ^1B diabatic state. The CNNC dihedral angle and both R_{NC} distances are varied independently, all other coordinates are optimized with C_2 symmetry constraints. The distance between two contour lines is 5 kcal/mol, all energies being relative to $N_2 + 2CH_3\cdot$. The locations and energies of some critical points are shown on the map. The *dotted line* encloses the region where $|\Delta E(S_0 - S_1)| < 5$ kcal/mol. Distances in bohr, angles in degree

minimum for $R_{N'C'} = R_{N''C''} = 2.75$ bohr, 72.2 kcal/mol above the ground state: by relaxing the planarity constraint for the CNNC skeleton, one finds that this is actually a saddle point, because torsion leads to stabilization of the excited state. Dissociation of one N—C bond on the S_1 surface requires to overcome a barrier, the top of which corresponds approximately to the vertical transition energy (87.9 kcal/mol): this process may therefore take place with excitation wavelengths lower than 325 nm. The outcome would be excited $CH_3NN\cdot$, certainly a very short lived entity. The irregularities in

contour levels of Fig. 5 around $R_{NC} = 4$ bohr are due to the sudden switch to a linear geometry of the outgoing $CH_3NN\cdot$ fragment. Simultaneous dissociation of the two N—C bonds leads to excited N_2, which is too high in energy to be of interest at ordinary wavelengths.

The preferred path in the excited state, and the only accessible one with $\lambda > 325$ nm, is torsion about the N—N bond. The ^1B diabatic surface as a function of the twisting angle and of the R_{NN} bond length (C_2 symmetry is imposed) is shown in Fig. 6. The dashed line indicates the crossing seam with the ^1A surface. It should be noted that the intersection takes place on one side of the valley which connects the cis and trans isomers: the lowest energy path does not lead through it; however, the lowest point of intersection, 73.7 kcal/mol above the ground state, is below the vertical excitation energy. Moreover, in a wider region around CNNC = 90°, the two PES are very close to each other: this is shown in Fig. 6 by dotted contours which correspond to $S_0 - S_1$ energy differences $\Delta E = \pm 5$ kcal/mol. A similar picture is obtained by varying symmetrically both NNC angles instead of R_{NN}. In contrast, changing the R_{NC} distances is not sufficient to meet the crossing seam, as shown in Fig. 7: the quasidegeneracy region ($|\Delta E| < 5$ kcal/mol) is wide enough to cross the lowest energy path. Fast IC is therefore expected at twisted geometries. The slope of the S_1 PES is steep nowhere, with the trans isomer being more stable than the cis one by about 7 kcal/mol and the relative minimum being located at CNNC = 130°: this shape of the PES may result in slightly unequal isomerization quantum yields, $\Phi_{cis\rightarrow trans} > \Phi_{trans\rightarrow cis}$.

5 Conclusions

The construction of PES for describing chemical reactions is a demanding task. Photochemistry poses peculiar problems, not only because two or more electronic states and their couplings must be considered: with respect to thermal reactions, higher energies are involved; therefore, it is necessary to sample wider regions of the nuclear coordinates' space and more reactive channels. In this study we have tackled such problems in the specific case of azomethane photochemistry, aiming at a suitable compromise between accuracy and completeness of the PES.

The natural continuation of this work is a dynamical treatment of the processes set off by excitation of azomethane. Classical trajectories with surface hopping have been run on the PES presented here and the analysis of the results is in progress. Some preliminary conclusions, in agreement with the qualitative considerations outlined in the previous section, can be put forward. IC is very fast (<1 ps) and almost half the trajectories, starting from the excited trans isomer, end up in the cis ground state. The dissociation of the N—C bonds needs much more time and takes place almost exclusively in the ground state. It may be described as sequential, but the second N—C bond breaks very soon after the first one because the methyldiazenyl radical is produced with a large excess of vibrational energy: this makes its observation as a photodissociation product quite unlikely.

Acknowledgements. This work was supported by grants of the Italian M.U.R.S.T. and C.N.R.

References

1. Engel PS (1980) Chem Rev 80: 99
2. Burton KA, Weisman RB (1990) J Am Chem Soc 112: 1804
3. Andrews BK, Burton KA, Weisman RB (1992) J Chem Phys 96: 1111
4. North SW, Longfellow CA, Lee YT (1993) J Chem Phys 99: 4423
5. Fairbrother DH, Dickens KA, Stair PC, Weitz E (1995) Chem Phys Lett 246: 513
6. Tully JC (1990) J Chem Phys 93: 1061
7. Ferretti A, Granucci G, Lami A, Persico M, Villani G (1996) J Chem Phys 104: 5517
8. Pacher T, Cederbaum LS, Köppel H (1993) Adv Chem Phys 84: 293
9. Persico M (1998) In: Schleyer PvR, Allinger NL, Clark T, Gasteiger J, Kollman PA, Schaefer HF III, Schreiner PR (eds) Encyclopedia of computational chemistry. Wiley, Chichester, p 852
10. Liu R, Cui Q, Dunn KM, Morokuma K (1996) J Chem Phys 105: 2333
11. Cattaneo P, Persico M (1997) Chem Phys 214: 49
12. Cattaneo P, Persico M (1998) Chem Phys Lett 289: 160
13. Huron B, Malrieu J-P, Rancurel P (1973) J Chem Phys 58: 5745
14. Cimiraglia R (1985) J Chem Phys 83: 1746
15. Cimiraglia R (1996) Int J Quantum Chem 60: 167
16. Angeli C, Cimiraglia R, Persico M, Toniolo A (1997) Theor Chem Acc 98: 57
17. Angeli C, Persico M (1997) Theor Chem Acc 98: 117
18. The version of the CIPSI package implemented by the Pisa and Ferrara research groups is available at the internet site www.dcci.unipi.it/Software.html
19. Persico M (1985) In: Rostas F (ed) Spectral line shapes, vol. 3. De Gruyter, Berlin, pp 587–613
20. Cimiraglia R, Malrieu J-P, Persico M, Spiegelmann F (1985) J Phys B 18: 3073
21. Hariharan PC, Pople JA (1973) Theor Chim Acta 28: 213
22. Dupuis M, Marquez A, Davidson ER (1995) HONDO95.3 form CHEM-station. IBM Corporation, Kingston, N.Y.
23. Krishnan R, Binkley JS, Seeger R, Pople JA (1980) J Chem Phys 72: 650
24. Angeli C, Cimiraglia R, Persico M, (1998) Theor Chem Acc 100: 324
25. Thompson AM, Goswami PC, Zimmermann GL (1979) J Phys Chem 83: 314
26. Engel PS (1976) J Am Chem Soc 98: 1972
27. Hu C-H, Schaefer HF III (1995) J Phys Chem 99: 7507
28. Vrábel I, Biskupič S, Staško A (1997) Theor Chem Acc 95: 201
29. Pamidimukkala KM, Rogers D, Skinner GB (1982) J Phys Chem Ref Data 11: 83
30. Hu C-H, Schaefer HF III (1994) J Chem Phys 101: 1289
31. Ács G, Péter A (1987) Int J Chem Kinet 19: 929
32. Almemingen A, Anfinsen IM, Haaland A (1970) Acta Chem Scand 24: 1230
33. Chang CH, Porter RF, Bauer SH (1970) J Am Chem Soc 92: 5313
34. Stevens JF, Curl RF, Engel PS (1979) J Phys Chem 83: 1432
35. Huber KP, Herzberg G (1979) Constants of diatomic molecules. Van Nostrand, New York